Spectrochimica Acta Part A: Molecular and Biomolecular Spectroscopy 297 (2023) 122752

Contents lists available at ScienceDirect

Spectrochimica Acta Part A:
Molecular and Biomolecular Spectroscopy

journal homepage: www.journals.elsevier.com/spectrochimica-acta-part-a-molecular-and-biomolecular-spectroscopy

Detection of pyrimidine-rich DNA sequences based on the formation of parallel and antiparallel triplex DNA and fluorescent silver nanoclusters

Juan Fernando García [a], David Reguera [a], Andrea Valls [a], Anna Aviñó [b], Arnau Dominguez [b], Ramon Eritja [b], Raimundo Gargallo [a,*]

[a] Dept. of Chemical Engineering and Analytical Chemistry, University of Barcelona, Marti i Franquès 1-11, E-08028 Barcelona, Spain
[b] Institute for Advanced Chemistry of Catalonia (IQAC-CSIC), CIBER-BBN, Jordi Girona 18-26, E-08034 Barcelona, Spain

HIGHLIGHTS

- Assessment of triplex DNA by means of spectroscopy and multivariate analysis.
- Development of silver nanoclusters sensors based on triplex DNA.
- Detection of pyrimidine-rich sequences at neutral pH by triplex DNA.

GRAPHICAL ABSTRACT

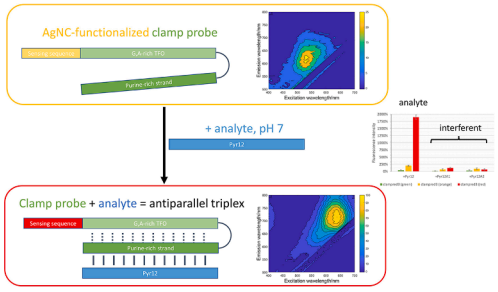

ARTICLE INFO

Keywords:
Nanoclusters
Parallel triplex DNA
Antiparallel triplex DNA
Silver nanoclusters
Detection
Fluorescence
Circular dichroism

ABSTRACT

In this work, the use of DNA-stabilized fluorescent silver nanoclusters for the detection of target pyrimidine-rich DNA sequences by formation of parallel and antiparallel triplex structures is studied by molecular fluorescence spectroscopy. In the case of parallel triplexes, the probe DNA fragments are Watson-Crick stabilized hairpins, and whereas in the case of antiparallel triplexes, the probe fragments are reverse-Hoogsteen clamps. In all cases, the formation of the triplex structures has been assessed by means of polyacrylamide gel electrophoresis, circular dichroism, and molecular fluorescence spectroscopies, as well as multivariate data analysis methods. The results have shown that it is possible the detection of pyrimidine-rich sequences with an acceptable selectivity by using the approach based on the formation of antiparallel triplex structures.

1. Introduction

The best-known DNA structure is the B-DNA, which is the right-handed double helix firstly proposed by Watson and Crick in 1953. Genomic research has revealed that around 98% of biological DNA is comprised of non-coding regions with important biological functions. These regions are characterized by repetitive DNA sequences that have the potential to fold into non-B DNA structures such as G-quadruplex [1,2], i-motif [3], or triplex [4], among others.

Triplex structures are formed by the addition of a triplex-forming oligonucleotide (TFO) strand to a duplex structure which, in turn, may be formed by two independent strands or by a single strand folded into a

* Corresponding author.
E-mail address: raimon_gargallo@ub.edu (R. Gargallo).

https://doi.org/10.1016/j.saa.2023.122752
Received 15 February 2023; Received in revised form 7 April 2023; Accepted 12 April 2023
Available online 17 April 2023

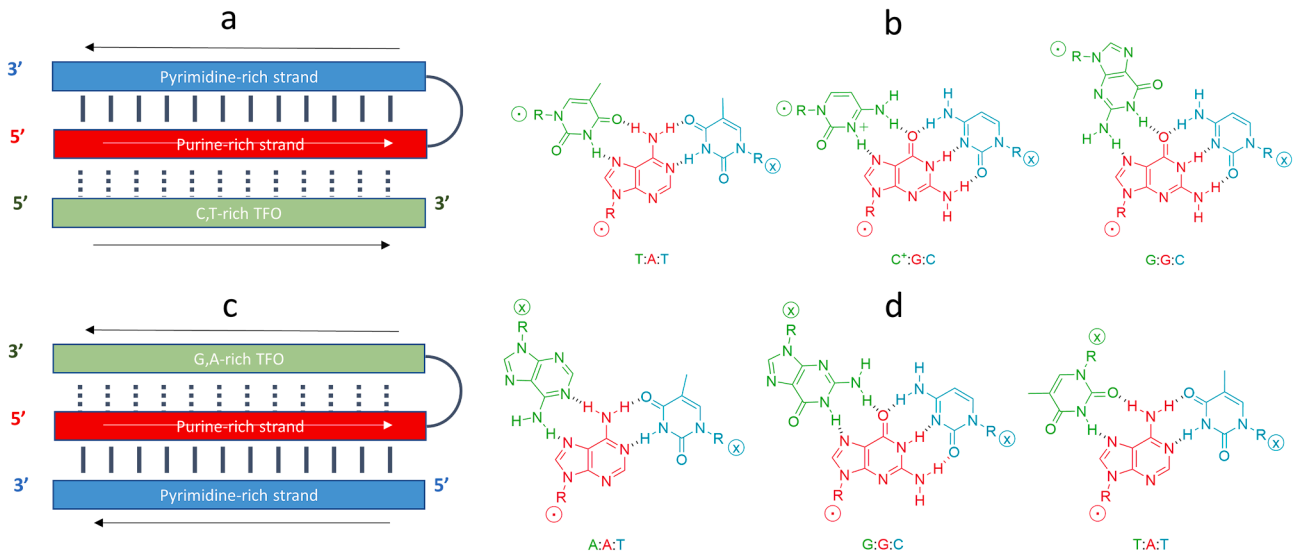

Fig. 1. Schemes of triplex structures. (a) Parallel triplex formed by a hairpin stabilized by Watson-Crick bonds and a C,T-rich strand (TFO). (b) Chemical structure and hydrogen bonding scheme of the triads present in parallel triplex DNA. (c) Scheme of the antiparallel triplex formed by a clamp sequence and a pyrimidine-rich strand. (d) Chemical structure and hydrogen bonding scheme of the triads present in antiparallel triplex DNA. In (a) and (c), solid lines indicate Watson-Crick hydrogen bonds, whereas dotted lines indicate non-Watson-Crick hydrogen bonds. Arrows indicate the 5′ to 3′ orientation of strands.

hairpin. In addition to the Watson-Crick base pairs observed within the duplex, Hoogsteen and reverse-Hoogsteen base pairs are formed between bases within TFO and bases within duplex [5]. To form stable triplex structures, the duplex should be formed by a purine-rich (i.e., with a high content of G and/or A bases) strand, paired to a pyrimidine-rich (i.e., with a high content of C and/or T bases) strand [6]. Depending on the orientation of the TFO with respect to the purine-rich strand within the duplex, triplex structures are classified into two main categories: parallel and antiparallel. In addition, it is possible to have a single stranded oligonucleotide to bind a duplex target sequence, or a clamp or hairpin binding a single stranded target sequence. In the parallel triplex, a pyrimidine-rich TFO binds in a parallel way to the purine-rich strand within the duplex (Fig. 1a), whereas in antiparallel triplex, a purine-rich oligonucleotide binds antiparallel to the purine-rich strand within the duplex (Fig. 1b). The protonation of cytosine bases within the pyrimidine rich TFO is required to form stable parallel triplexes. For this reason, the stability of these structures is pH-dependent being greater near the pK_a of cytosine (around 4.5). On the contrary, the formation of antiparallel triplex structures does not require protonation of any nitrogenous base, being its stability largely pH independent. In this work, two of the strands involved in the formation of either parallel or antiparallel triplex structures are linked by means of a short loop, forming a hairpin (Fig. 1a and c). This approach not only facilitates the experimental preparation of equimolar amounts of duplex and TFO strands, but also increases the stability of the final structures formed.

Fig. 1 *should be near here.*

In the case of antiparallel structures, this work uses the term “clamp” to refer to single-stranded hairpins formed by two antiparallel purine-rich tracts linked by a thymidine loop and bound by intramolecular reverse-Hoogsteen bonds. In the bibliography these clamps are known as Polypurine reverse-Hoogsteen hairpins (PPRH, [7,8]) but we prefer to name them as “clamp” to differentiate with the Watson-Crick hairpins that are used in this work for parallel triplex formation. The clamps (PPRH) can bind in a sequence-specific manner to pyrimidine-rich sequences by Watson–Crick bonds, thus forming an antiparallel triplex (Fig. 1c). These clamps have been described as gene silencing tools of several genes mainly involved in cancer with the capacity to produce strand displacement [9]. Additionally, they have been incorporated as probes in biosensors for the detection of miRNAs [10], and SARS-CoV-2 [7], among other applications.

Metal noble nanoclusters (NCs) have been suggested as one of the most important contributions of Nanotechnology to Nanomedicine due to their excellent physical and chemical properties [11,12]. NCs are tiny (below 2 nm) groups of a few metal atoms that have quantized molecule-like orbitals, enabling the existence of spectroscopic phenomena, such as fluorescence [1314]. Specifically, silver nanoclusters (AgNCs) prepared by reduction of silver ions in the presence of short DNA oligonucleotides have attracted a large interest as potential diagnostic tools for their tunable and high fluorescent properties, such as brightness, wide spectral range and photostability, as well as because of their good biocompatibility [15,16,17,18].

The presence of DNA strands enables the stabilization of AgNCs, preventing further aggregation into larger and non-fluorescent silver nanoparticles. Although many studies have been conducted trying to correlate the DNA sequences, their lengths, and their secondary structures with the fluorescence properties of AgNCs [19,20], research is still far to be completed [21,22]. It is known, for instance, that cytosine bases bind to silver species much stronger than other bases, such as guanine, adenine, or thymine. Hence, many of the published works about DNA-stabilized AgNCs deal with cytosine-rich sequences. However, the significance of the length and of the secondary structures of the DNA templates on the emission properties of the resulting AgNCs is still matter of research [23,24,25,26,27]. As example, some authors propose that i-motif structures, which are formed by cytosine-rich sequences at pH lower than 7, may stabilize AgNCs [28], where other authors propose that only neutral cytosine bases at pH 7.4 may stabilize AgNCs [20].

Whereas the application of hairpin stabilized AgNCs to Nanotechnology and analysis has been widely studied [29], the use of AgNCs stabilized by triplex structures has been studied in a few works. Ihara *et al.* [30] reported a method for stabilization of the parallel triplex DNA using Ag(I) ions. They found that Ag(I) ion could specifically displace an N3 proton of a cytosine in the C·G·C^+ base site of triplex DNA to form a new triplet (C·G·Ag·C), which would stabilize the parallel-motif triplex even at neutral pH. This approach was later used by Feng *et al.* to design site-specific, and homogeneous AgNCs with high stability against salt using parallel triplex DNA as templates. They observe that Ag_2 clusters could be obtained in the very position of CG·C^+ site of triplex DNA [31]. Recently, the fluorescence of AgNCs encapsulated inside the loop of parallel triplexes was studied as a function of pH and the presence of duplex DNA [32]. Finally, Lu *et al.* proposed the detection of miRNAs

Table 1
DNA sequences studied in this work. Bases in bold and underlined are those corresponding to the loop. The stretch in red denotes the sensing sequence.

DNA name	Sequence (5′ →3′)	Role
H28	AGG AAG GAA AAG **TTTT** CTT TTC CTT CCT	Probe
H28m	AGG AAG GAA AAG **CCCC** CTT TTC CTT CCT	Probe
H28red3	AGG AAG GAA AAG **TTTT** CTT TTC CTT CCT **CCC TAA CTC CCC**	Probe
H28red5	**CCC TAA CTC CCC** AGG AAG GAA AAG **TTTT** CTT TTC CTT CCT	Probe
Clampmod	GAA AAG GAA GGA **CCCCC** AGG AAG GAA AAG	Probe
Clampred3	GAA AAG GAA GGA **TTTTT** AGG AAG GAA AAG **CCC TAA CTC CCC**	Probe
Clampred5	**CCC TAA CTC CCC** GAA AAG GAA GGA **TTTTT** AGG AAG GAA AAG	Probe
Pyr12	TCC TTC CTT TTC	Analyte
Pyr12A1	TCC TTC CTT ATC	Interferent
Pyr12A2	TCA TTC CTT ATC	Interferent
CtrlDuplexred3	GAA AAG GAA GGA **CCC TAA CTC CCC**	Probe
CC5red3	GGA AAA GAA AGG **TTTT** GGA AAG AAA AGG **CCC TAA CTC CCC**	Probe
CC5target	CCT TTC TTT TCC	Analyte

using triplex molecular beacons and silver nanoclusters [33].

Concerning antiparallel triplex, to our knowledge very few works deal with AgNCs involved in the formation of antiparallel triplex based on the use of clamps. Wang *et al.* developed a sensor for melanine using an approach based on antiparallel triplex structures [34]. This approach has the advantage of being developed at neutral pH, like *in vivo* conditions. Also working at neutral and basic pH values, Nagda *et al.* studied the stabilization of AgNCs by triplex structures, and the formation of DNA nanostructures [32].

In this work, the formation of parallel and antiparallel triplex structures has been assessed firstly by means of several experimental methods. Then, the fluorescent properties of the AgNCs stabilized by modified hairpins and clamps have been studied. Finally, the changes of the fluorescence of these AgNCs have been monitored in presence of pyrimidine-rich sequences. The hypothesis behind this work is that the fluorescence of the AgNCs stabilized by any of the probes (hairpins or clamps) would be modified dramatically in presence of the target TFO, making possible the detection of this sequence. The obtained results have shown that the use of AgNCs and antiparallel triplex structures may be a way to detect pyrimidine-rich sequences at neutral pH. This is an attractive application of this methodology as it has been recently shown that the genome of viruses may contain several pyrimidine-rich stretches suitable for designing triplex-forming hairpins with analytical or therapeutic purposes [7].

2. Experimental section

2.1. Reagents

The DNA oligonucleotides (Table 1) were provided by Sigma-Aldrich (Merck KGaA, Germany). The integrity of all DNA oligonucleotides was checked by means of MALDI-TOF Mass Spectrometry. DNA strand concentration was determined by absorbance measurements (260 nm) at 90 °C using the extinction coefficients calculated using the nearest-neighbor method as implemented on the OligoCalc webpage [35]. Sodium acetate (pH 4.9) and potassium phosphate (pH 7.4) buffers, $AgNO_3$ and $NaBH_4$ were purchased from Merck KGaA. MilliQ (Merck Millipore, MA, USA) water was used in all experiments.

Table 1 *should be near here.*

The h28 sequence is the non-modified DNA hairpin that will target Pyr12 sequence to yield a parallel triplex structure, according to scheme shown in Fig. 1a. The h28m sequence shows a modified loop where thymines have been replaced by cytosines, which are known to be the nitrogenous bases that better stabilize AgNCs [36]. Both, the h28red3 and h28red5 sequences incorporate a 12-nucleotides sensing sequence (CCC TAA CTC CCC) at the 3′ or 5′ ends, respectively, which has been shown to stabilize fluorescent AgNCs [37]. All these four hairpins may form parallel triplex structures with the Pyr12 sequence.

The clampmod sequence is a purine-rich strand that incorporates a short stretch of five cytosine bases. This sequence may produce an antiparallel triplex structure upon hybridization with the Pyr12 sequence, according to the scheme shown in Fig. 1c. The stretch of cytosine bases will be then located at the loop of the resulting antiparallel triplex. As in the case of the hairpins, clampred3 and clampred5 incorporate the sensing sequence at the 3′ and 5′ ends, respectively. Pyr12A1 and Pyr12A2 show one and two mismatches upon formation of triplex structures. CtrDuplexred3 is a sequence that may form a Watson-Crick intermolecular duplex with Pyr12. Finally, the sequences CC5red3 and CC5Target are oligonucleotides designed for the detection of SARS-CoV-2 RNA and they have been used to confirm some of the results shown in this work.

2.2. Procedures

2.2.1. PAGE measurements

Polyacrylamide gel electrophoresis assays were carried out mixing the hairpin or clamp probes with the corresponding TFO (1:1 or 1:2 ratio) or each one of them alone in a 50 mM phosphate buffer at pH 7.2 containing 10 mM $MgCl_2$ and 100 mM NaCl with a concentration of 24 μM per oligonucleotide. The samples (20 μl) supplemented with 5 % glycerol were incubated 30 min at 37 °C. Electrophoresis was performed on a nondenaturing 8 % polyacrylamide gel containing 10 mM $MgCl_2$, 5 % glycerol and 50 mM phosphate buffer (pH 7.2). The gels were run at 110 mV (10 °C) for 3 h using a running phosphate buffer (pH 7.2) solution of 50 mM and 10 mM $MgCl_2$. A mixture of xylene cyanol and bromophenol blue (1:1) was used as a dye to follow the progression of the gel. Finally, the gels were stained using Stains-all.

2.2.2. Preparation of silver nanoclusters

DNA-stabilized AgNCs were synthesized using the procedures described previously [38]. In a vial containing the appropriate medium (acetate or phosphate buffer, magnesium chloride if needed), an aliquot of the oligonucleotide stock solution was introduced. A certain volume of $AgNO_3$ was then added to achieve a 1:6 DNA:Ag(I) ratio, the mixture was shaken, and allowed to stand for 15 min at room temperature and in the dark. Then, freshly prepared $NaBH_4$ was added to the DNA:Ag(I) mixture up to a 1:6:6 DNA:Ag(I):borohydride ratio, and the solution was stirred vigorously for 1 min. The synthesized DNA-AgNCs were stored at 4 °C in the dark for one hour before measurement. The $AgNO_3$ stock solution was prepared by dissolving in a 10 mL volumetric flask the mass of $AgNO_3$ required to obtain a 0.1 M concentration solution. A $1 \cdot 10^{-3}$ M $AgNO_3$ solution was obtained through a dilution cascade, which was stored at room temperature in an amber volumetric flask to prevent oxidation. The $NaBH_4$ stock solution was prepared daily by dissolving the appropriate amount of solid $NaBH_4$ in a 25 mL volumetric flask to obtain a 0.1 M solution. From this, a $1 \cdot 10^{-3}$ M $NaBH_4$ solution was obtained by dilution, which was kept on ice until use.

2.3. Instruments and apparatus

Absorbance spectra were recorded with an Agilent 8453 diode array spectrophotometer. Hellma quartz cells (10 mm path length, 400 and 1500 μl volume, Germany) were used. CD spectra were recorded with a Jasco J-815 (MD, USA) spectropolarimeter equipped with a Peltier accessory for temperature control. Hellma quartz cells (10 mm path length, 3000 μl volume) were used. CD monitored melting experiments were measured with a temperature ramp of 0.6 $^{o}C \cdot min^{-1}$. In addition, some measurements were also recorded by using molecular absorption spectroscopy from 15 to 70 °C with a ramp 2 $^{o}C \cdot min^{-1}$ each 3 min. In both cases, the determined melting temperatures (T_m) values were similar.

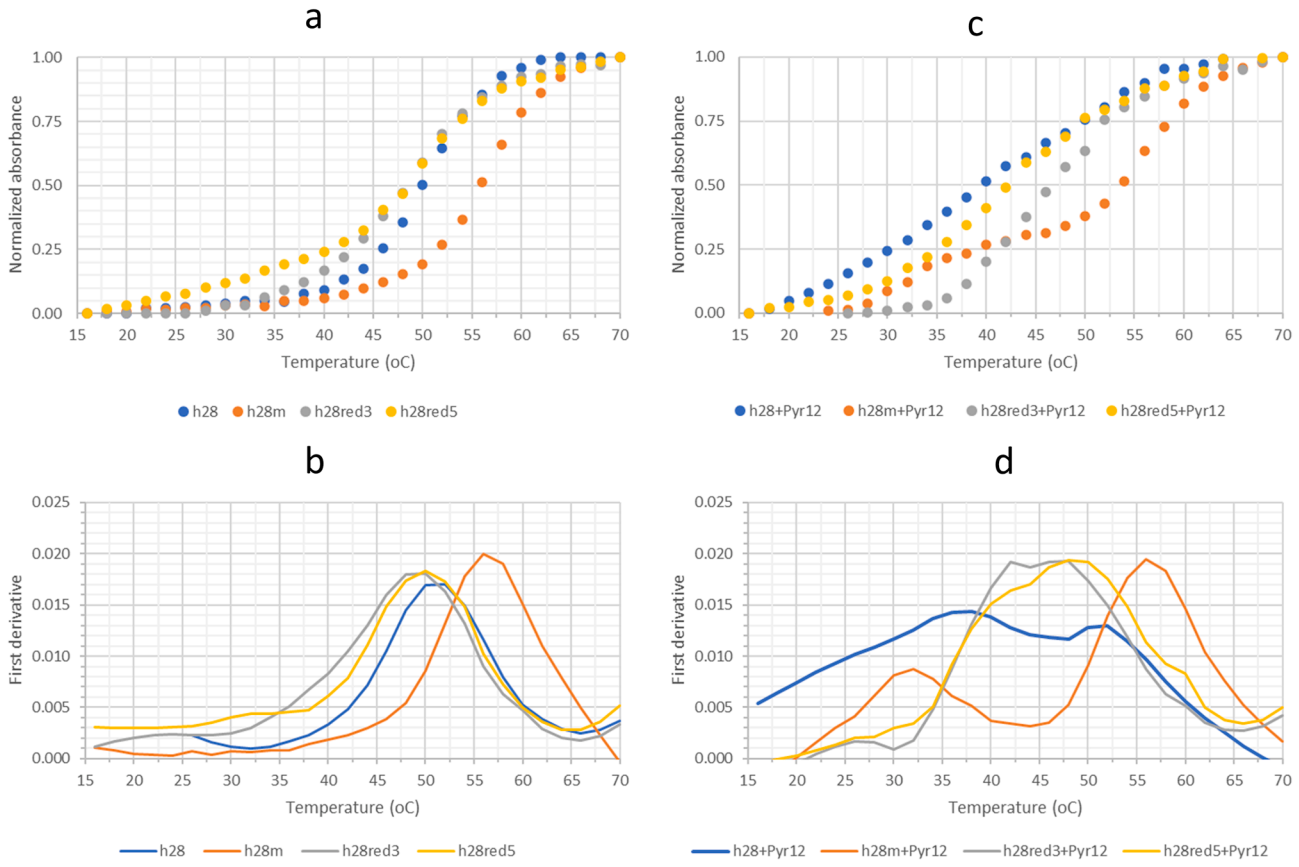

Fig. 2. Melting experiments of hairpins (a, b) and Pyr12:hairpin mixtures (c, d). (a) and (c) are the normalized melting curves, (b) and (d) are the first derivatives of the melting curves. Experimental conditions of the melting experiment were 20 mM acetate buffer, pH 4.9, 2 μM hairpin, and 2 μM Pyr12.

Fluorescence experiments were monitored using an AB2 Aminco-Bowman (Thermo Fisher, MA, USA) spectrofluorimeter. For most of the measurements, excitation and emission slits were set to 4 nm, and voltage of the photomultiplier was set within the range 800–1000 V. A Hellma quartz cell (2 × 10-mm path length, and 400 μl volume) was used. 3D excitation-emission maps (EEMs) were measured from 400 to 700 nm (excitation), and from 500 to 800 nm (emission). The Rayleigh scattering was removed by replacing the original values by an estimate of the background fluorescence signal. This estimate was calculated from the mean value of a wide region of the EEM where no fluorescence was observed, and later addition of random noise. Finally, the EEM was smoothed by applying a Savitzky-Golay filter. All these procedures were done using in-house developed Matlab® (The MathWorks, Inc., MA, USA) routines. The following spectral ranges were considered along the manuscript: green (501–565 nm), yellow (566–590 nm), orange (591–625 nm), and red (626–740 nm).

Atomic Force Microscopy (AFM) analysis was performed using a commercial atomic force microscope (Dimension 3100 with electronics Nanoscope V, Bruker, USA) in tapping mode using a rectangular-shaped silicon cantilever with a pyramidal tip curvature of 10 nm and a nominal spring constant of 15 $N{\cdot}m^{-1}$.

2.4. Multivariate analysis

Multivariate analysis uses data recorded at more than one channel. In the case of molecular absorption or CD spectroscopies, a channel corresponds to a wavelength at which absorbance or ellipticity was measured along the considered experiment. Accordingly, either absorbance or CD spectra recorded along meltings were arranged in a matrix **D**, the dimensions of which were *m* spectra × *n* channels. For instrumental techniques that provide a linear signal *vs.* concentration response, it is possible to decompose this matrix **D** according to the equation:

$$\boldsymbol{D} = \boldsymbol{C}{\cdot}\boldsymbol{S} + \boldsymbol{E} \tag{1}$$

C is a matrix that contains the distribution diagram for all the components present along the titration. The dimensions of matrix **C** are $m \times nc$, being *nc* the proposed number of components. **S** is the matrix that contains the absorbance or CD spectra of each one of these components, also called pure spectra. The dimensions of **S** are $nc \times n$. Finally, **E** is the matrix ($m \times n$) of experimental data not explained by the multiplication of **C** by **S**. For the appropriate number of components, data in **E** should be randomly distributed.

In this work, decomposition of matrix **D** has been done by using the Multivariate Curve Resolution based on Alternating Least Squares (MCR-ALS) procedure. Briefly, the decomposition of **D** according to Eq. (1) is accomplished by an iterative mode at the end of which matrices **C** and **S** are calculated. The calculation implies the application of several constraints to the values contained in matrix **C**, like the closure concentration (i.e., the sum of concentrations of all components is forced to be constant) or non-negativity of concentration values. A deeper description of this procedure, as well as its many applications in Chemistry and Biophysics, may be found in previous works [39,40,41,42].

3. Results and discussion

First, the formation of parallel triplex structures at pH 4.9 involving Watson-Crick hairpins and the pyrimidine-rich sequence Pyr12 will be assessed, and fluorescence properties of the AgNCs stabilized by these hairpins will be studied, both in absence and presence of the Pyr12 sequence. A similar rationale will be applied for antiparallel triplex at

Table 2
Thermodynamic parameters calculated from the melting curves at pH 4.9 of hairpins and 1:1 hairpin:Pyr12 mixtures [44]. Experimental conditions of the experiments were 20 mM acetate buffer, pH 4.9, 2 μM hairpin and 2 μM Pyr12.

DNA sequence	Transition from the hairpin to the unfolded strand				Transition from the triplex to the mixture of hairpin and Pyr12			
	ΔH^o (kJ·mol^{-1})	ΔS^o (J·K^{-1}·mol^{-1})	ΔG^o_{15} (kJ·mol^{-1})	T_m (°C)	ΔH^o (kJ·mol^{-1})	ΔS^o (J·K^{-1}·mol^{-1})	ΔG^o_{15} (kJ·mol^{-1})	T_m (°C)
h28	−236 ± 6	−729 ± 11	−26 ± 2	50.8 ± 0.5	−170 ± 11	−438 ± 30	−43 ± 3	33.1 ± 1.2
h28m	−233 ± 11	−707 ± 34	−29 ± 2	56.3 ± 0.1	−209 ± 19	−580 ± 64	−42 ± 1	28.2 ± 0.3
h28red3	−147 ± 16	−453 ± 52	−16 ± 2	50.2 ± 1.1	−173 ± 19	−442 ± 59	−45 ± 2	37.4 ± 0.6
h28red5	−154 ± 5	−478 ± 16	−16 ± 1	49.6 ± 0.8	−192 ± 26	−512 ± 81	−45 ± 2	33.6 ± 0.9

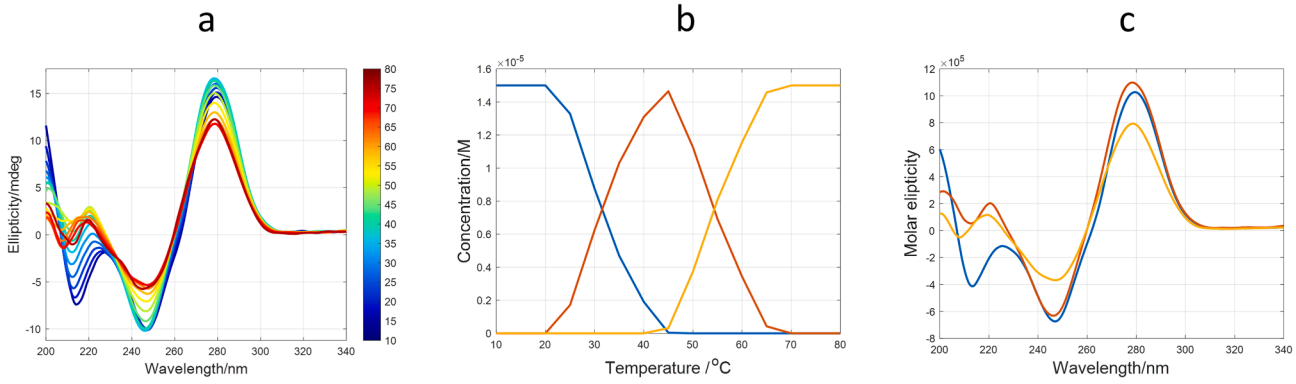

Fig. 3. Melting of the 1:1 h28:Pyr12mixture at pH 4.9. (a) Experimental CD spectra. (b) MCR-ALS calculated distribution diagram. (c) MCR-ALS calculated pure spectra. Blue: parallel triplex formed by h28 and Pyr12, red: mixture of the hairpin h28 and Pyr12, orange: mixture of unfolded h28 and Pyr12. Experimental conditions of the melting experiment were 20 mM acetate buffer, pH 4.9, 15 μM h28, and 15 μM Pyr12.

pH 7.4.

3.1. Assessment of the formation of parallel triplex structures

Spectroscopically monitored melting experiments at pH 4.9 were performed to assess the formation of the parallel triplex structures from the 1:1 mixture of the corresponding hairpins and Pyr12.

First, the melting process of the h28 sequence was studied by means of molecular absorption spectroscopy (Fig. 2a and b). A single transition was observed at 260 nm, which could be fitted to a two-state transition with a T_m equal to 50.8 ± 0.5 °C (Table 2). According to OligoCalc [35] and Nupack [43], the intermolecular B-DNA duplex with the same sequence as of h28 (i.e., without the T_4 loop) would unfold with a T_m around 36–40 °C. Therefore, a dramatic stabilization was obtained when working with hairpin instead than with the mixture of the complementary strands. Similar T_m values were determined for h28red3 and h28red5, showing that the addition of the sensing sequence had scarce effect on the thermal stability of the hairpin (Fig. 2b). On the other hand, the melting temperature of h28m was slightly higher (56.3 ± 0.1 °C), revealing a slight stabilizing effect due to the C_4 loop. This is probably related to the formation of one additional C·C$^+$ base pair, such as those observed in i-motif structures. Thermodynamic parameters for the folding of hairpins were calculated using a previously published procedure [26]. It was observed that the changes in enthalpy and entropy were significantly smaller in the case of h28red3 and h28red5 than for the h28 and h28m sequences. This fact may be related to a smaller cooperativity of the folding process when the sensing sequence was attached at either the 3′ or 5′ end of the hairpin. On the other hand, no variation of the absorbance at 260 nm was observed in the case of the Pyr12 sequence (data not shown, which was related to the absence of a highly ordered structure at low temperature. A CD-monitored melting experiment was also carried out to confirm this point (Fig. S1).

Next, the formation of the parallel triplex structures was assessed. The absorbance traces at 260 nm are shown in Fig. 2c. The mixture of h28m + Pyr12 clearly showed two clear transitions with maximum values of the first derivative at 32 and 56 °C (Fig. 2d). These would correspond to the disruption of the parallel triplex and the unfolding of the hairpin, respectively. The melting of the 1:1 h28:Pyr12 mixture also showed two maximum values of the first derivative around 37 and 52 °C, respectively. For the h28red3:Pyr12 and h28red5:Pyr12 mixtures the resolution of the two unfolding steps was not as clear as in the cases of the h28:Pyr12 or h28m:Pyr12 mixtures.

To gain additional information, CD-monitored melting experiments were carried out. As example, Fig. 3a shows the CD spectra measured along the melting of the 1:1 h28:Pyr12 mixture at pH 4.9. The disruption of the triplex structure is clearly observed in the region around 210 nm. To gain insight into the nature of the transitions observed, multivariate analysis was done by means of Multivariate Curve Resolution - Alternating Least Squares (MCR-ALS) procedure [41]. This mathematical deconvolution confirmed the existence of two transitions, i.e., three components were present along the melting. Additional analysis was done considering two or four components, and the best results (both in terms of fitting as in the chemical interpretation) were obtained when three components were considered. The distribution diagram and pure spectrum for each one of these components were calculated (Fig. 3b and 3c, respectively). The first transition, which takes place from 20 to 45 °C, approximately, is characterized by a T_m value around 34 °C. According to the spectral changes observed at 210 nm, this transition was explained as the release of the Pyr12 strand from the triplex structure. The second transition, which takes place from 45 to 70 °C, approximately, was explained as the result of the unfolding of a B-DNA hairpin structure. From absorbance or ellipticity *versus* temperature curves, thermodynamic parameters for the disruption of the triplex structure were calculated (Table 2) [26].

A similar procedure was used to analyze the data recorded along the melting experiments of mixtures involving Pyr12 and h28m, h28red3 or h28red5. For the h28m:Pyr12 mixture, the determined T_m value for the release of the TFO was slightly lower than in the case of the triplex involving h28 (28.2 *vs.* 33.1 °C), which shows a destabilizing effect of the C5 loop on the triplex. As the hairpin formed by h28m is more stable

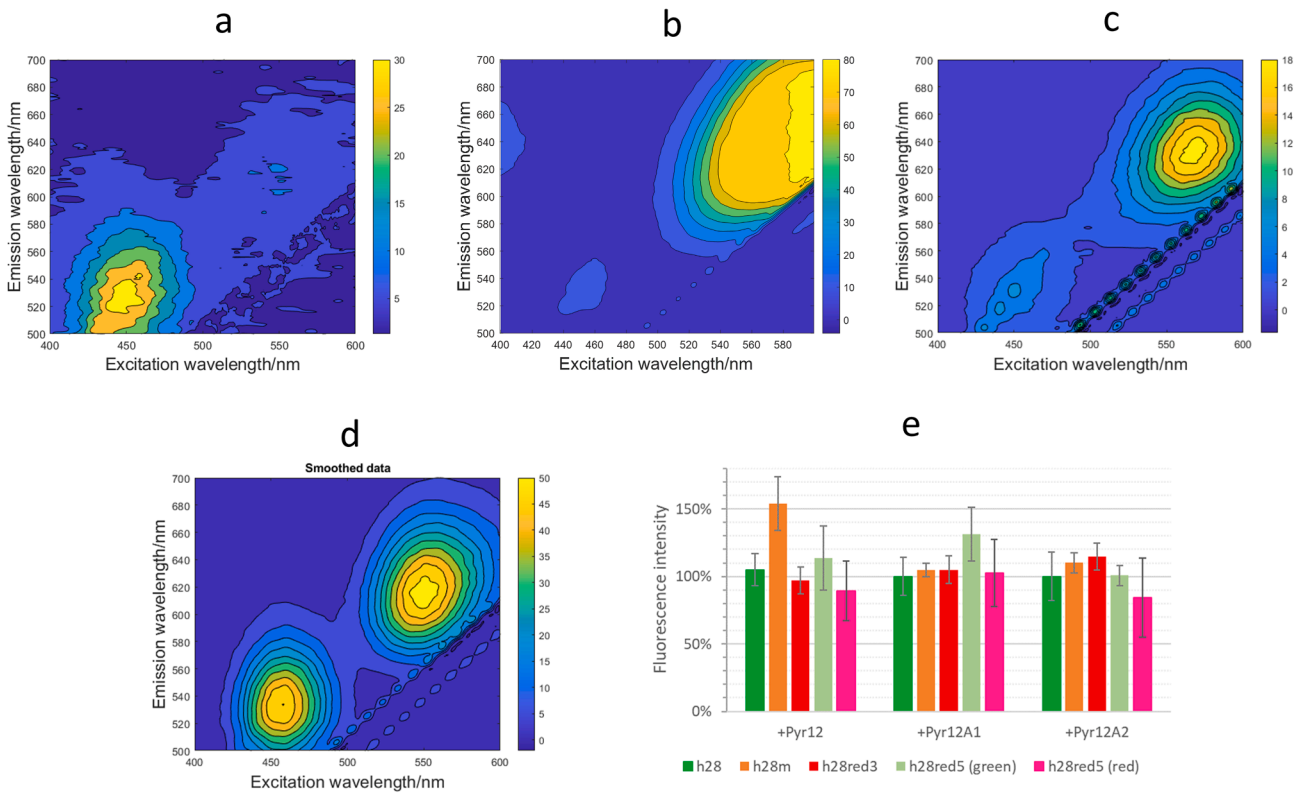

Fig. 4. EEM of h28 (a), h28m (b), h28red3 (c), h28red5 (d) and variation of fluorescence intensity of the most characteristics emission bands of AgNCs stabilized by h28, h28m, h28red3, and h28red5 in presence of Pyr12, and interferents (e). In all cases, hairpin and target concentration was 5 μM, Ag(I) and borohydride concentration was 30 μM, 15 °C, 20 mM acetate buffer, pH 4.9. The voltage of the detector was set to 1100 (h28), 600 (h28m), and 800 V (h28red3 and h28red5).

than that formed by h28, and this additional stabilization could be related to the formation of intramolecular C·C$^+$ base pairs, it could be expected that the addition of positive charge would destabilize the triplex structure. In the case of h28red3, the disruption of the triplex structure takes place at higher temperatures than in the case of h28 and h28m. Therefore, it seems that the sensing sequence may play a certain role on the stabilization of the triplex, especially when is attached to the 3′-end (h28red3; 37.4 *vs.* 33.1 °C).

3.2. *Fluorescence properties of AgNCs stabilized by parallel triplexes*

Once the formation of parallel triplex structures was assessed, the formation of DNA-templated silver nanoclusters by these hairpin-forming sequences was studied. The synthesis was done according to the procedure described above. AgNCs stabilized by the hairpins were studied firstly by means of Atomic Force Microscopy. AFM images (Fig. S3) indicated that the AgNCs stabilized by hairpins were spherical particles within a certain range of diameters.

EEM spectra of the AgNCs formed by these hairpin-forming sequences at pH 4.9 are shown in Fig. 4. AgNCs synthesized using h28 showed weak fluorescence in the green region, as the voltage of the detector was set to 1100 V (Fig. 4a). On the contrary, AgNCs stabilized by the h28m sequence showed strong red fluorescence signal at 650 nm (voltage set to 600 V), in addition to a weaker fluorescence in the green region (Fig. 4b). These spectral trends are in line with those shown for hairpins of 7 base-pair stems [45]. In this sense, the fluorescence of hairpin stabilized AgNCs has also been discussed in terms of the intramolecular hairpin *vs.* intermolecular dimer equilibrium [24]. Hence it has been hypothesized that the dimer structure is more suitable to encapsulate orange emissive AgNCs, while the hairpin structure would enable the generation of red-emissive AgNCs. The strong red fluorescence of AgNCs stabilized by h28m suggests the existence of a cluster of Ag atoms stabilized by the cytosines of the loop. Other authors have proposed the formation of a head-to-head ensemble of two hairpins, bridged by the AgNC, which would emit fluorescence around 620 nm [46]. AgNCs stabilized by the hairpin h28red3 showed orange fluorescence at 630 nm (Fig. 4c). On the other hand, the sequence h28red5 produced two clear fluorescence bands with similar intensities in the green (530 nm) and red (620 nm) regions, which could be related to the existence of two different AgNCs (Fig. 4d). According to previous works, the emission wavelength could also be indicative of the number of Ag atoms within each cluster [47]. Hence, emission in the green and orange-red regions would correspond to nanoclusters involving four and six Ag atoms, respectively.

The hypothesis behind this work is that the fluorescence of the AgNCs stabilized by any of the probes would be modified dramatically in presence of the target TFO (the Pyr12 sequence), making possible the detection of this sequence. Therefore, the effect of the addition of this sequence to the AgNCs stabilized by the hairpins was studied (Fig. 4e). Upon addition of Pyr12 up to 1:1 h28:Pyr12 ratio, the green emission of h28 does not show any variation and neither appears new fluorescence in other spectral regions. Upon addition of Pyr12 up to 1:1 hairpin:Pyr12 ratio, the orange emission of h28m increased slightly, but no new fluorescence bands appeared in the spectral range studied (500–800 nm). Addition of sequences that do not form the perfect triplex (Pyr12A1 and Pyr12A2) produced no changes on the fluorescence of the probe. For AgNCs stabilized by h28red3 or h28red5, no clear changes were observed upon addition of any DNA sequence. Therefore, it was clear that, upon formation of the parallel triplex structures, any clear change of the analytical signal that could be used to quantify, or even detect, Pyr12 was observed. Hence, an alternative approach based on the use of antiparallel triplexes was investigated.

3.3. *Assessment of the formation of antiparallel triplex structures*

The detection of the Pyr12 sequence was then investigated based on

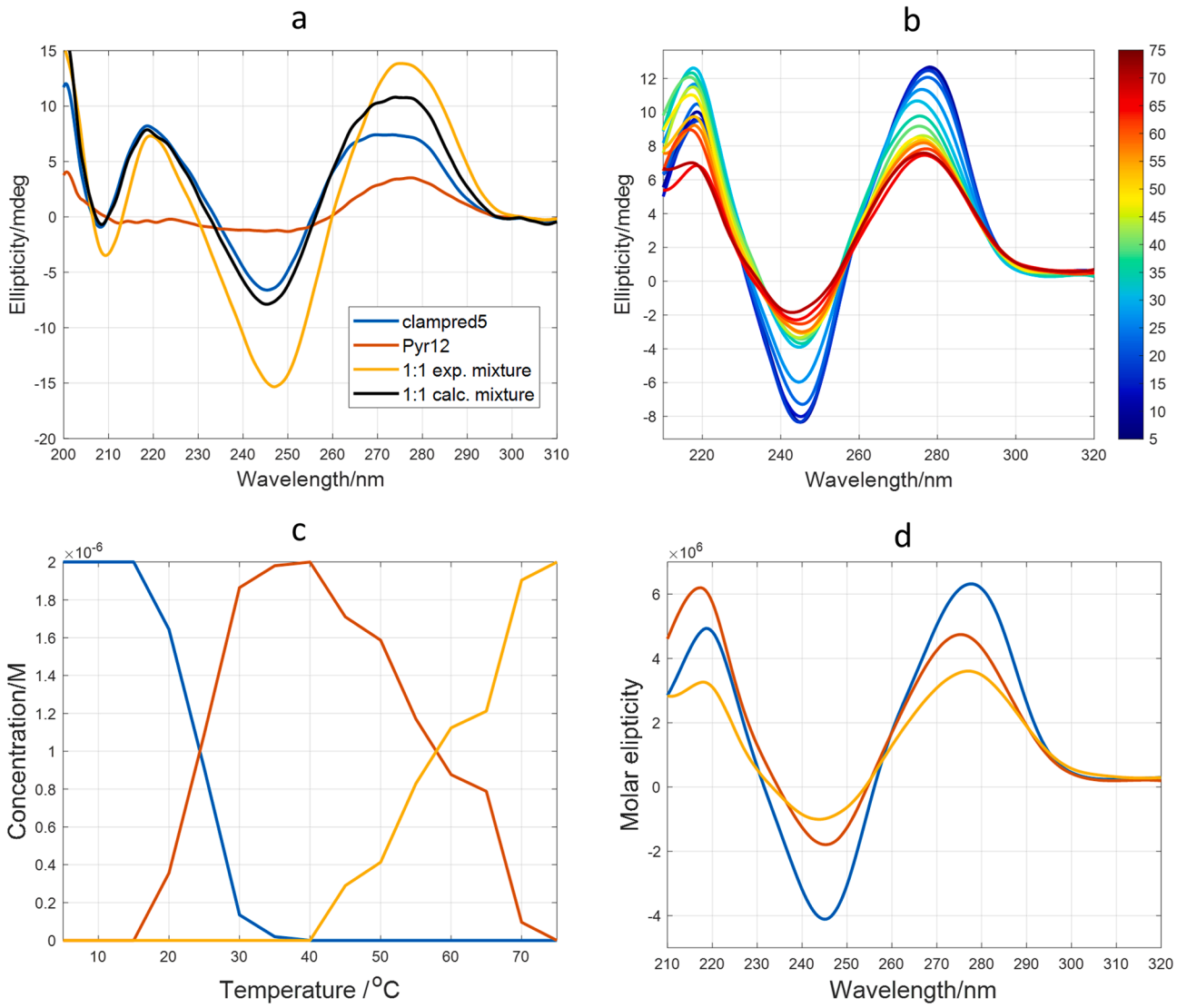

Fig. 5. (a) CD spectra of Pyr12 (red), clampred5 (blue), and the experimental (yellow), and calculated (black) 1:1 mixtures. Experimental conditions of the measurements were 20 mM phosphate buffer, pH 7.4, 20 mM magnesium chloride, 2 μM clampred5, and 2 μM Pyr12. (b) Experimental CD spectra measured along the melting of the 1:1 clampred5:Pyr12mixture at pH 7.4. (c) MCR-ALS calculated distribution diagram. (d) MCR-ALS calculated pure spectra. In (c) and (d): blue corresponds to the antiparallel triplex formed by clampred5 and Pyr12 (stabilized by both Watson-Crick and Hoogsteen base pairs). Red: mixture of an intramolecular structure formed by clampred5 and Pyr12. Orange: mixture of unfolded clampred5 and Pyr12. Experimental conditions of the melting experiment in b-d were 20 mM phosphate buffer, pH 7.4, 100 mM NaCl, 2 μM clampred5, and 2 μM Pyr12.

the formation of antiparallel triplexes by the TFO and a fluorescent-labelled clamp (Table 1). First, the formation of the triplex structures was assessed by means of spectroscopy and PAGE experiments.

Fig. 5a shows the CD spectra of Pyr12, clampred5, and of the 1:1 mixture of both strands (20 mM phosphate buffer, and 20 mM magnesium chloride). As described above, Pyr12 does not fold into any highly ordered structure at these conditions, and the shape of its CD spectrum, which only shows a positive band around 275 nm, reflects this low degree of order. The spectrum of clampred5, on the other hand, shows well defined positive and negative bands. The measured spectrum of the mixture is compared with that calculated from the mathematical sum of the CD spectra of Pyr12 and clampred5. The shape of the experimental and calculated spectra is different, suggesting the formation of intermolecular structures in the mixture of Pyr12 and clampred5.

It is known that absorbance changes associated to the unfolding of antiparallel triplex structures are less pronounced that those observed along the unfolding of parallel triplex structures [48,49], making very difficult the detection of antiparallel triplex with this method. Therefore, CD spectroscopy, that is more sensitive to the DNA conformational changes, was used instead to monitor the unfolding of a 1:1 mixture of Pyr12 and clampred5.

First, melting experiments were carried out in a 20 mM phosphate buffer, and 20 mM magnesium chloride. However, it was observed the presence of a precipitate at temperatures higher than 50 °C, approximately. This fact is in line with the structural role of magnesium ions on the stabilization of triplex structures [50,51]. Upon unfolding of the initial folded structure, magnesium ions would be released from it and subsequent precipitation as hydroxide or phosphate would take place [52]. Therefore, melting experiments were carried out in absence of magnesium chloride. Fig. 5b shows the CD monitored melting of the 1:1 mixture of clampred5 and Pyr12. At 5 °C, CD spectrum shows positive signals at 218 and 278 nm, and a negative signal at 245 nm. Upon heating, the intensities of these bands decreased and small shifts of the band at 278 nm were observed concomitantly. From the CD signals at 245 and 278 nm it may be observed a relatively sharp transition between 20 and 40 °C, followed by a smooth transition at higher temperatures.

MCR-ALS was applied to the analysis of this data set. It was found that two transitions, i.e., three species, were needed to explain the data,

Table 3
Thermodynamic parameters calculated from the melting curves at pH 7.4 of 1:1 clamps:Pyr12 mixtures [44]. Experimental conditions of the experiments were 20 mM phosphate buffer, pH 7.4, 2 μM clamp and 2 μM Pyr12.

DNA sequence	Transition from the ordered structure to the unfolded strands (intramolecular folding)			
	ΔH^o ($kJ \cdot mol^{-1}$)	ΔS^o ($J \cdot K^{-1} \cdot mol^{-1}$)	ΔG^o_{15} ($kJ \cdot mol^{-1}$)	T_m (°C)
Clampred3	−116 ± 10	−384 ± 22	−5.3 ± 1.0	28.8 ± 1.2
Clampred5	−138 ± 8	−458 ± 16	−6.6 ± 1.5	29.5 ± 0.8

and the corresponding distribution diagram and pure spectra are shown in Fig. 5c and 5d (Table 3). In a complementary experiment, the melting of the 1:1 mixture of Pyr12 and CtrlDuplexred3 was done. Only one transition was observed with a T_m value equal to 24 ± 1 °C (Fig. S2), corresponding to the breaking of the duplex structure stabilized by Watson-Crick bonds. Therefore, the first transition observed in Fig. 5c, which takes place around 25 °C, would involve the breaking of the Watson-Crick base pairs. As the stability of the reverse Hoogsteen base pairs that stabilize the triplex structure is lower than that of Watson-Crick base pairs, it is expected that the entire triplex structure unfolds completely in one single step with a T_m value around 25 °C. The second transition would be related to the smooth unfolding of the intramolecular species formed by clampred5, according to Nupack calculations [43] (Fig. S4). Two additional melting experiments were done for the 1:1 mixtures of CtrlDuplexred3:Pyr12 and clampred5:Pyr12 in 20 mM phosphate buffer and 100 mM NaCl. It was observed a shift of the transition to 37 °C (data not shown), in agreement with the stabilizing effect of cations on DNA duplex and triplex structures. Similar results were obtained from the melting experiments of the 1:1 mixtures involving clampmod and clampred3 with Pyr12.

According to the results obtained, at 15 °C the antiparallel triplex is not fully formed and a small fraction of Pyr12 would remain unhybridized. To assess the formation of the antiparallel triplex structures, PAGE experiments were carried out (Fig. 6). For clampred3 and clampred5 a shifted band with less mobility was observed when Pyr12 was added compared with the control clamps in agreement with the formation of a triplex structure. Yet, no shifted band was observed for clampmod even with an excess of TFO (1:2) indicating that this sequence cannot form the corresponding triplex. Furthermore, at a 1:1 ratio all clampred5 is forming triplex, since only one shifted band can be observed. However, for clampred3 two bands can be seen, suggesting that the binding of clampred5 to Pyr12 could be slightly stronger than that for clampred3.

3.4. Fluorescence properties of modified clamps

Once the formation of antiparallel triplex structures was assessed, the fluorescence properties of the AgNCs stabilized by the clamps were studied (Fig. 7). All three clamps showed intense fluorescence emission signal around 630 nm. Upon addition of the target Pyr12 sequence, clampred3 showed the appearance of an intense red fluorescence around 700 nm (Fig. 7e). In the case of clampred5, an increase of the fluorescence at 700 nm is also observed in presence of the Pyr12 sequence, but the change is not as dramatic as in the case of clampred3.

AgNCs stabilized by clampred3 were studied by means of AFM. Images in Fig. S3 indicated the formation of spherical particles with a size range from 47 to 297 nm.

The changes of the fluorescence signal of the probe (clampred3 or clampred5) are probably due, at least partially, to the formation of the Watson-Crick stabilized duplex between the purine strand of the probes and the pyrimidine-rich target sequence. To study this possibility, the fluorescence of the AgNCs stabilized by the CtrlDuplexred3 in absence and presence of the target Pyr12 sequence was done (Fig. S5). It was observed a small increase of the fluorescence in the red region, which suggests that the appearance of the red fluorescence in the case of antiparallel triplex was also partially due to the formation of the duplex structure.

Interestingly, other interferent species present do not produce the appearance of the red fluorescence in the case of clampred3. To gain insight into the selectivity of AgNCs stabilized by clampred3, a new

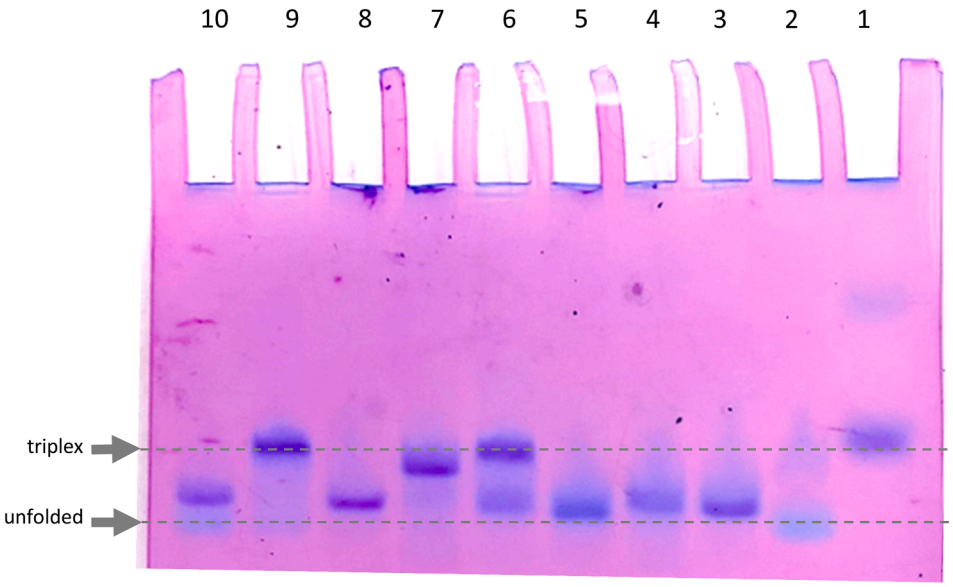

Fig. 6. PAGE analysis carried out at pH 7.4 for clamps and mixtures with Pyr12. Experimental conditions are described in the corresponding section.

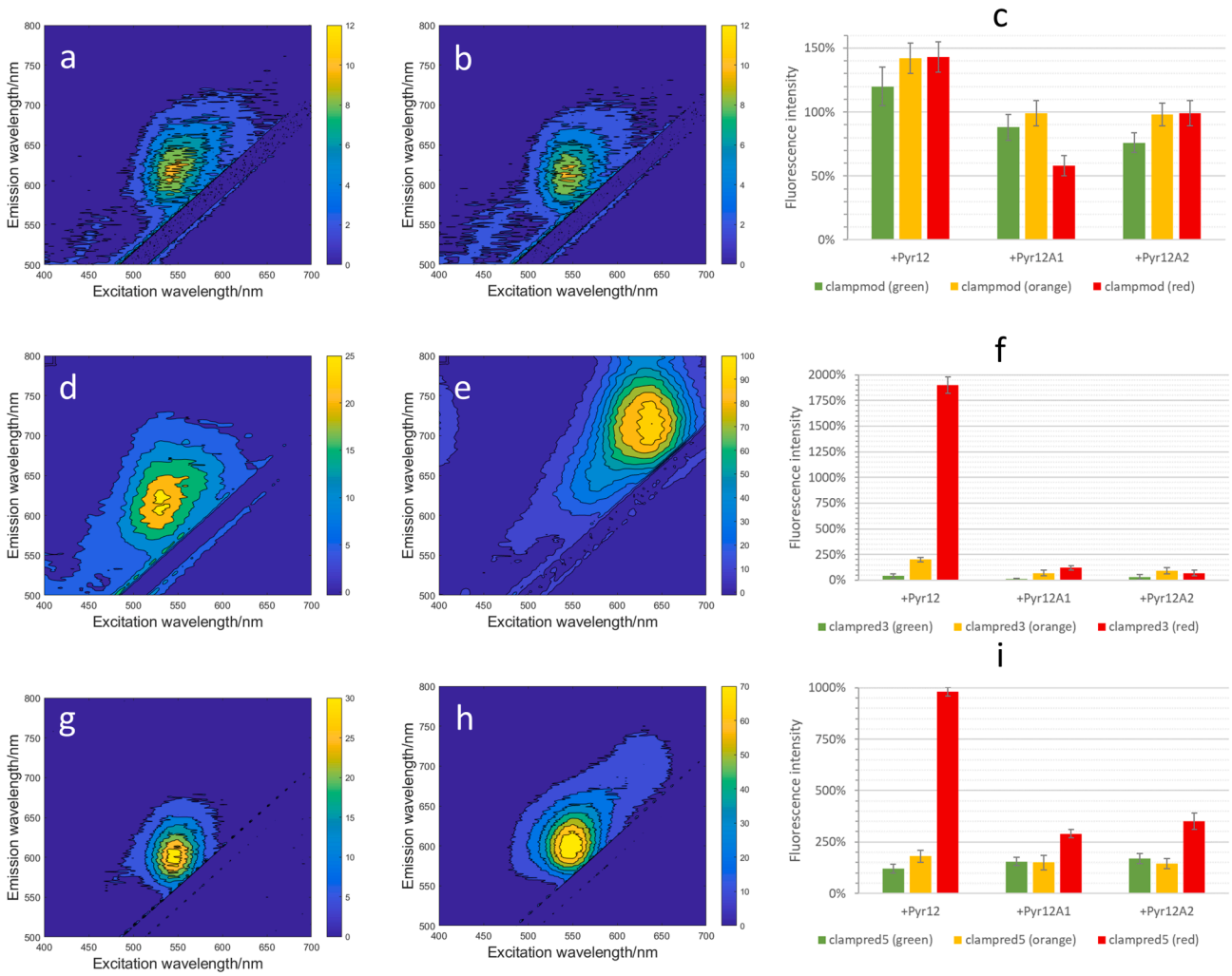

Fig. 7. EEM of AgNCs stabilized by clampmod (a), clampred3 (d), and clampred5 (g). EEM of the 1:1 mixtures of Pyr12 with clampmod (b), clampred3 (e), and clampred5 (h). Relative change of fluorescence of the AgNCs stabilized by clampmod (c), clampred3 (f), and clampred5 (i) in presence of the analyte (Pyr12) and several interferents. In all cases, clamp, target and interferent concentration was 5 μM, Ag(I) and borohydride concentration was 30 μM, 15 °C, 20 mM magnesium chloride, 20 mM phosphate buffer, pH 7.4.

experiment was carried out to study the influence of interferents, as well as the effect of aging time (Fig. 8). It was observed that the fluorescence of the probe (i.e., AgNCs stabilized by clampred3) increased smoothly over time. The fluorescence of the 1:1 mixture of the probe and the perfect matching TFO (Pyr12) produced the observed increase of fluorescence in the red region, being the maximum fluorescence reached around 5 h, approximately. In the presence of the Pyr12A1 sequence, which presents one mismatch, the measured fluorescence was half that observed in the presence of the perfect TFO. In the case of Pyr12A2 sequence, which presents two mismatches, the recorded fluorescence was like that of the probe, i.e., no triplex was formed. Finally, the fluorescence of the mixtures of Pyr12 and Pyr12A1 (or Pyr12A2) showed an intermediate behavior, which could be related to a small interferent effect of these sequences.

Finally, a calibration curve was constructed for a probe consisting of clampred3 4 μM and different concentrations of Pyr12. The fluorescence was measured at 720 nm, being the voltage of the detector set to 950 V (Fig. S6). In these conditions, the lowest concentration of Pyr12 that could be detected was 0.5 μM.

The proposed methodology was also tested with an additional modified clamp (CC5red3), which is being studied for the detection of SARS-CoV-2 by means of a strategy based on the formation of antiparallel triplex [7]. First, the formation of antiparallel triplex with the corresponding target sequence CC5target was assessed (Fig. S7a). The measured CD spectrum of the mixture showed similar trends to those observed for the mixture of clampred5 and Pyr12. Also, the measured spectrum was different from the calculated CD spectrum of the mixture. Finally, the EEM maps of the AgNCs stabilized by CC5red3 showed the clear appearance of red fluorescence in presence of the target sequence (Fig. S7b and S7c), as in the case of clampred3 or clampred5 in presence of their target analyte Pyr12.

4. Discussion

The detection of single stranded sequences by hybridization to AgNCs stabilized by the complementary sequence to obtain the duplex has been already described [53]. In the present work, the goal was the detection of target cytosine-rich DNA fragments based on the formation of triplex structures. This strategy may show additional advantages to the application of the duplex-based approach. Hence, a higher degree of selectivity may be obtained due to the combined interaction of both Watson-Crick and reverse-Hoogsteen purine strands with the target viral RNA.

Two different approaches, based on the formation of either parallel or antiparallel triplexes have been studied. In all cases, the formation of triplex structures has been assessed by means of spectroscopic methods.

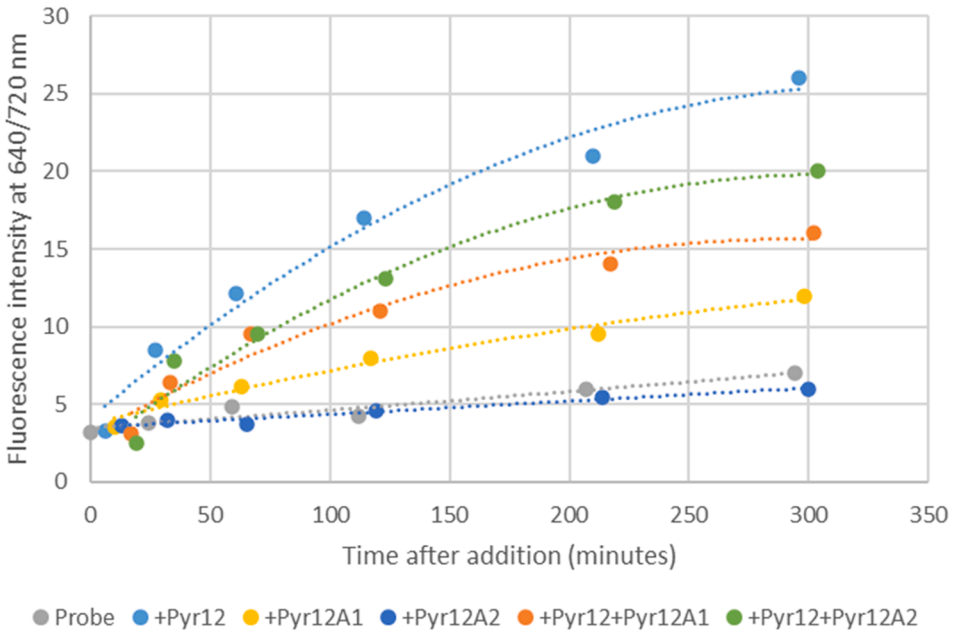

Fig. 8. Time dependence of fluorescence of clampred3-stabilized AgNCs in presence of different targets. In all cases, clampred3 and target concentration was 5 μM, Ag(I) and borohydride concentration was 30 μM, 15 °C, 20 mM magnesium chloride, 20 mM phosphate buffer, pH 7.4.

In the case of parallel triplexes at pH 4.9, the probe consisted of AgNCs stabilized by hairpins, whereas clamps were used as DNA stabilizing strands in the case of antiparallel triplexes at pH 7.4. The results have shown that detection based on the formation of antiparallel triplexes could be possible when the sensing sequence was attached to the 3′ end of the clamp.

Other authors have used hairpins for the detection of DNA or RNA, but their approaches were different to those shown here. For instance, Xia *et al.* designed hairpins where AgNCs were attached to the 3′ and 5′ ends, like in this work, whereas the stem and part of the loop was the recognition site for a miRNA [54]. Upon hybridization, the hairpin was unfolded, AgNCs were released, and a fall of fluorescence was observed. Also, Feng *et al.* used pre-formed parallel triplex structures to react with Ag(I) and later reduction with borohydride. The hypothesis behind that work is that site-specific formation of fluorescent AgNCs could be carried out by reducing Ag(I) ions *in situ* in the C:G·C^+ triplet [31]. In their work, they did not observe fluorescence for the AgNCs stabilized by the hairpin, and only green fluorescence was seen after incubation for three days of the mixture of parallel triplex, Ag(I) and borohydride. In our case, we observed fast-developing green fluorescence for the AgNCs stabilized by h28, but any change was seen after immediate addition of the target Pyr12. Later, these authors proposed the use of AgNcs stabilized by parallel triplex structures to detect thiols by using a combination of electrochemistry and fluorescence techniques [55].

The strategy based on the formation of parallel triplex structures was shown not to be adequate to obtain any spectroscopic signal that could be of analytical interest for the detection of Pyr12. The reason behind this fact could be that DNAs used in this study showed cytosine-rich sequences that could form i-motif or i-motif-like structures that could compete with the formation of the triplex structures [56]. Also, it could be that the formation of the triplex from the hairpin and TFO did not produce dramatic changes in the environment of fluorescent AgNCs. In this case, the appearance of a fluorescence signal in the red region in the case of clampred3 at pH 7.4 would be related to a conformational change of the probe in presence of Pyr12.

Not only for AgNCs stabilized by clamps at pH 7.4, but also for those stabilized by hairpins at pH 4.9 it was shown that the position of the sensing sequence 5′- CCC TAA CTC CCC-3′ at the 5′ or 3′ ends of clamps or hairpin may produce different fluorescent characteristics. It has been shown that the properties of AgNCs such as stability, fluorescence and so on are highly dependent on the nature and structure of the template molecules used for nanocluster synthesis [24], like the polarity of the hosting DNA sequence plays an important role on the fluorescence of AgNCs [56].

The results obtained in this work pointed out to the detection of pyrimidine-rich sequences by detecting the formation of triplex structures. Therefore, the approach may be also applied for the detection of these structures, which assessment is not straightforward from spectroscopic measurements.

5. Conclusions

In this work, the application of a strategy based on the formation of triplex structures for the detection of pyrimidine-rich sequences has been investigated. It has been shown that different fluorescence bands may be obtained depending on the position of the cytosine-rich sensing fragment. The addition of this sensing element does not affect dramatically to the formation of the parallel triplex at pH 5. However, little changes in fluorescence of the probes were observed upon formation of the parallel triplex structures, which hinders its application as sensors. A different picture was obtained when working with clamps able to form antiparallel triplex structures with the target pyrimidine-rich sequence. In this case, it was observed that the attachment of the labelled sequence at the 3′ end produced the appearance of strong fluorescence signal at 720 nm in presence of the target sequence, with relative high selectivity.

CRediT authorship contribution statement

Juan Fernando García: Investigation, Formal analysis. **David Reguera:** Investigation, Formal analysis. **Andrea Valls:** Investigation, Formal analysis. **Anna Aviñó:** Investigation, Resources. **Arnau Dominguez:** Investigation, Formal analysis. **Ramon Eritja:** Methodology, Resources, Writing – review & editing, Funding acquisition. **Raimundo Gargallo:** Methodology, Software, Writing – review & editing, Supervision, Project administration.

Declaration of Competing Interest

The authors declare that they have no known competing financial interests or personal relationships that could have appeared to influence the work reported in this paper.

Data availability

Data will be made available on request.

Acknowledgments

We thank funding from the Spanish *Ministerio de Ciencia e Innovación* (PID2019-107158GB-I00 and PID2020-118145RB-I00) and *La Marató* de TV3 Foundation (202110-30). Javier Pacheco (University of Barcelona) is also thanked for carrying out some of the fluorescence experiments.

Appendix A. Supplementary material

Supplementary data to this article can be found online at https://doi.org/10.1016/j.saa.2023.122752.

References

[1] S. Neidle, Quadruplex nucleic acids as novel therapeutic targets, J. Med. Chem. 59 (2016) 5987–6011, https://doi.org/10.1021/acs.jmedchem.5b01835.
[2] L. Liu, W. Liu, K. Wang, B. Zhu, X. Xia, L. Ji, Z. Mao, Quantitative detection of G-quadruplex DNA in live cells based on photon counts and complex structure discrimination, Angew. Chem. Int. Ed. 59 (2020) 9719–9726, https://doi.org/10.1002/anie.202002422.
[3] S.L. Brown, S. Kendrick, The I-motif as a molecular target: more than a complementary DNA secondary structure, Pharmaceuticals. 14 (2021) 1–25, https://doi.org/10.3390/ph14020096.
[4] A. Jain, G. Wang, K.M. Vasquez, DNA triple helices: biological consequences and therapeutic potential, Biochimie. 90 (2008) 1117–1130, https://doi.org/10.1016/j.biochi.2008.02.011.
[5] K.M. Vasquez, P.M. Glazer, Triplex-forming oligonucleotides: principles and applications, Q. Rev. Biophys. 35 (2002) 89–107, https://doi.org/10.1017/S0033583502003773.
[6] R. Eritja, Nucleic acids triple helices, in: R. Eritja (Ed.), Nucleic Acids Chemistry. Modifications and Conjugates for Biomedicine and Nanotechnology, Walter de Gruyter GmbH, Berlin, 2021, pp. 187–230.
[7] A. Aviñó, C. Cuestas-Ayllón, M. Gutiérrez-Capitán, L. Vilaplana, V. Grazu, V. Noé, E. Balada, A. Baldi, A.J. Félix, E. Aubets, S. Valiuska, A. Domínguez, R. Gargallo, R. Eritja, M.-P. Marco, C. Fernández-Sánchez, J. Martínez de la Fuente, C.J. Ciudad, Detection of SARS-CoV-2 virus by triplex enhanced nucleic acid detection assay (TENADA), Int. J. Mol. Sci. 23 (2022) 15258, https://doi.org/10.3390/ijms232315258.
[8] S. Valiuska, A.M. Psaras, V. Noé, T.A. Brooks, C.J. Ciudad, Targeting MYC regulation with polypurine reverse hoogsteen oligonucleotides, Int. J. Mol. Sci. 24 (2022) 378, https://doi.org/10.3390/ijms24010378.
[9] V. Noé, E. Aubets, A.J. Félix, C.J. Ciudad, Nucleic acids therapeutics using PolyPurine Reverse Hoogsteen hairpins, Biochem. Pharmacol. 189 (2021), 114371, https://doi.org/10.1016/j.bcp.2020.114371.
[10] A. Aviñó, C.S. Huertas, L.M. Lechuga, R. Eritja, Sensitive and label-free detection of miRNA-145 by triplex formation, Anal. Bioanal. Chem. 408 (2016) 885–893, https://doi.org/10.1007/s00216-015-9180-6.
[11] J.P. Wilcoxon, B.L. Abrams, Synthesis, structure and properties of metal nanoclusters, Chem. Soc. Rev. 35 (2006) 1162–1194, https://doi.org/10.1039/B517312B.
[12] X. Liu, F. Meng, R. Sun, K. Wang, Z. Yu, P. Miao, Three-dimensional bipedal DNA walker enabled logic gates responding to telomerase and miRNA, Chem. Commun. 57 (2021) 2629–2632, https://doi.org/10.1039/D0CC08089F.
[13] J.T. Petty, J. Zheng, N.V. Hud, R.M. Dickson, DNA-templated Ag nanocluster formation, J. Am. Chem. Soc. 126 (2004) 5207–5212, https://doi.org/10.1021/ja031931o.
[14] J. Sharma, H.-C. Yeh, H. Yoo, J.H. Werner, J.S. Martinez, A complementary palette of fluorescent silver nanoclusters, Chem. Commun. 46 (2010) 3280, https://doi.org/10.1039/b927268b.
[15] I. Díez, R.H.A. Ras, Fluorescent silver nanoclusters, Nanoscale. 3 (2011) 1963, https://doi.org/10.1039/c1nr00006c.
[16] B. Han, E. Wang, DNA-templated fluorescent silver nanoclusters, Anal. Bioanal. Chem. 402 (2012) 129–138, https://doi.org/10.1007/s00216-011-5307-6.
[17] Z. Yuan, Y.-C.-Y.-C. Chen, H. Wen Li, H.-T.-H.-T. Chang, H.-W. Li, H.-T.-H.-T. Chang, Fluorescent silver nanoclusters stabilized by DNA scaffolds, Chem. Commun. (Camb). 50 (2014) 9800–9815, https://doi.org/10.1039/c4cc02981j.
[18] J. Xu, X. Zhu, X. Zhou, F. Yeasmin, C. Ma, Recent advances in the bioanalytical and biomedical applications of DNA-templated silver nanoclusters, Trends Anal. Chem. 124 (2020), 115786, https://doi.org/10.1016/j.trac.2019.115786.
[19] Y. Teng, X. Yang, L. Han, E. Wang, The relationship between DNA sequences and oligonucleotide-templated silver nanoclusters and their fluorescence properties, Chem. – Euro. J. 20 (2014) 1111–1115, https://doi.org/10.1002/chem.201301473.
[20] A. Latorre, A. Somoza, Á. Somoza, DNA-mediated silver nanoclusters: synthesis, properties and applications, ChemBioChem. 13 (2012) 951–958, https://doi.org/10.1002/cbic.201200053.
[21] S.Y. New, S.T. Lee, X.D. Su, DNA-templated silver nanoclusters: structural correlation and fluorescence modulation, Nanoscale. 8 (2016) 17729–17746, https://doi.org/10.1039/C6NR05872H.
[22] J. Ma, H. Niu, S. Gu, The spatial organization of trace silver atoms on a DNA template, RSC Adv. 11 (2021) 1153–1163, https://doi.org/10.1039/D0RA08066G.
[23] B. Sengupta, C. Corley, K. Cobb, A. Saracino, S. Jockusch, DNA scaffolded silver clusters: a critical study, Molecules. 21 (2016) 1–15, https://doi.org/10.3390/molecules21020216.
[24] P. Shah, S.W. Choi, R. Nagda, R. Geczy, S.K. Cho, Y.J. Bhang, T.-H. Kim, T.Y. Song, P.H. Lee, J.-H. Kang, P.W. Thulstrup, M.J. Bjerrum, I.L. Jung, S.W. Yang, The structural shift of a DNA template between a hairpin and a dimer tunes the emission color of DNA-templated AgNCs, Nanoscale. 10 (2018) 20717–20722, https://doi.org/10.1039/C8NR06186F.
[25] J.T. Petty, O.O. Sergev, D.A. Nicholson, P.M. Goodwin, B. Giri, D.R. McMullan, A silver cluster–DNA equilibrium, Anal. Chem. 85 (2013) 9868–9876, https://doi.org/10.1021/ac4028559.
[26] P. Shah, A. Rørvig-Lund, S. Ben Chaabane, P.W. Thulstrup, H.G. Kjaergaard, E. Fron, J. Hofkens, S.W. Yang, T. Vosch, Design aspects of bright red emissive silver nanoclusters/DNA probes for MicroRNA detection, ACS Nano. 6 (2012) 8803–8814, https://doi.org/10.1021/nn302633q.
[27] R. Nagda, P. Shah, C.S. Lee, S. Park, S.W. Yang, Structural influence on the post-clustering stability of DNA/AgNCs fluorescence, Nanomaterials. 9 (2019) 667, https://doi.org/10.3390/nano9050667.
[28] T. Li, N. He, J. Wang, S. Li, Y. Deng, Z. Wang, A. Rørvig-Lund, S.W. Yang, N. N. Degtyareva, J.T. Petty, T. Goodson, Y. Song, Y. Wang, D. Liu, L. Jiang, Effects of the i-motif DNA loop on the fluorescence of silver nanoclusters, RSC Adv. 6 (2016) 22839–22844, https://doi.org/10.1039/C5RA22489F.
[29] R. Abolhasan, A. Mehdizadeh, M.R. Rashidi, L. Aghebati-Maleki, M. Yousefi, Application of hairpin DNA-based biosensors with various signal amplification strategies in clinical diagnosis, Biosens. Bioelectron. 129 (2019) 164–174, https://doi.org/10.1016/j.bios.2019.01.008.
[30] T. Ihara, T. Ishii, N. Araki, A.W. Wilson, A. Jyo, Silver ion unusually stabilizes the structure of a parallel-motif DNA triplex, J. Am. Chem. Soc. 131 (2009) 3826–3827, https://doi.org/10.1021/ja809702n.
[31] L. Feng, Z. Huang, J. Ren, X. Qu, Toward site-specific, homogeneous and highly stable fluorescent silver nanoclusters fabrication on triplex DNA scaffolds, Nucl. Acids Res. 40 (2012) e122–e, https://doi.org/10.1093/nar/gks387.
[32] R. Nagda, S. Park, I.L. Jung, K. Nam, H.C. Yadavalli, Y.M. Kim, K. Yang, J. Kang, P. W. Thulstrup, M.J. Bjerrum, M. Cho, T.-H. Kim, Y.H. Roh, P. Shah, S.W. Yang, Silver nanoclusters serve as fluorescent rivets linking hoogsteen triplex DNA and hairpin-loop DNA structures, ACS Nano. 16 (2022) 13211–13222, https://doi.org/10.1021/acsnano.2c06631.
[33] S. Lu, S. Wang, J. Zhao, J. Sun, X. Yang, Classical triplex molecular beacons for MicroRNA-21 and vascular endothelial growth factor detection, ACS Sens. 3 (2018) 2438–2445, https://doi.org/10.1021/acssensors.8b00996.
[34] Y. Wang, Q. Sun, L. Zhu, J. Zhang, F. Wang, L. Lu, H. Yu, Z. Xu, W. Zhang, Triplex molecular beacons for sensitive recognition of melamine based on abasic-site-containing DNA and fluorescent silver nanoclusters, Chem Commun. 51 (2015) 7958–7961, https://doi.org/10.1039/C5CC01660F.
[35] W.A. Kibbe, Oligo Calc: an online oligonucleotides properties calculator, Nucl. Acids Res. 35 (2007) W43–W46.
[36] C.M. Ritchie, K.R. Johnsen, J.R. Kiser, Y. Antoku, R.M. Dickson, J.T. Petty, Ag nanocluster formation using a cytosine oligonucleotide template, J. Phys. Chem. C. 111 (2007) 175–181, https://doi.org/10.1021/jp0648487.
[37] C.I. Richards, S. Choi, J.C. Hsiang, Y. Antoku, T. Vosch, A. Bongiorno, Y.L. Tzeng, R.M. Dickson, Oligonucleotide-stabilized Ag nanocluster fluorophores, J. Am. Chem. Soc. 130 (2008) 5038–5039, https://doi.org/10.1021/ja8005644.
[38] A. de la Hoz, A. Navarro, A. Aviñó, R. Eritja, R. Gargallo, Studies on the interactions of Ag (I) with DNA and their implication on the DNA-templated synthesis of silver nanoclusters and on the interaction with, RSC Adv. 11 (2021) 9029–9042, https://doi.org/10.1039/D1RA00194A.
[39] P. Kumar, A. Verma, S. Maiti, R. Gargallo, S. Chowdhury, Tetraplex DNA transitions within the human c-myc promoter detected by multivariate curve resolution of fluorescence resonance energy transfer, Biochemistry. 44 (2005), https://doi.org/10.1021/bi051452x.
[40] R. Gargallo, R. Tauler, A. Izquierdo-Ridorsa, Acid-base and copper(II) complexation equilibria of poly(inosinic)-poly(cytidylic), Biopolymers. 42 (1997) 271–283.
[41] J. Jaumot, R. Tauler, R. Gargallo, Exploratory data analysis of DNA microarrays by multivariate curve resolution, Anal. Biochem. 358 (2006) 76–89, https://doi.org/10.1016/j.ab.2006.07.028.
[42] S. Benabou, R. Ferreira, A. Aviñó, C. González, S. Lyonnais, M. Solà, R. Eritja, J. Jaumot, R. Gargallo, Solution equilibria of cytosine- and guanine-rich sequences near the promoter region of the n-myc gene that contain stable hairpins within lateral loops, Biochim. Biophys. Acta Gen. Subj. 2014 (1840) 41–52, https://doi.org/10.1016/j.bbagen.2013.08.028.

[43] J.N. Zadeh, C.D. Steenberg, J.S. Bois, B.R. Wolfe, M.B. Pierce, A.R. Khan, R. M. Dirks, N.A. Pierce, NUPACK: analysis and design of nucleic acid systems, J. Comput. Chem. 32 (2011) 170–173, https://doi.org/10.1002/JCC.21596.
[44] A. Dillen, W. Vandezande, D. Daems, J. Lammertyn, Unraveling the effect of the aptamer complementary element on the performance of duplexed aptamers: a thermodynamic study, Anal. Bioanal. Chem. 413 (2021) 4739–4750, https://doi.org/10.1007/s00216-021-03444-y.
[45] P.R. O'Neill, L.R. Velazquez, D.G. Dunn, E.G. Gwinn, D.K. Fygenson, Hairpins with poly-C loops stabilize four types of fluorescent Ag $_n$:DNA, J. Phys. Chem. C. 113 (2009) 4229–4233, https://doi.org/10.1021/jp809274m.
[46] R. Geczy, N.J. Christensen, K.K. Rasmussen, I. Kálomista, M.K. Tiwari, P. Shah, S. W. Yang, M.J. Bjerrum, P.W. Thulstrup, Formation and structure of fluorescent silver nanoclusters at interfacial binding sites facilitating oligomerization of DNA hairpins, Angew. Chem. – Int. Ed. 59 (2020) 16091–16097, https://doi.org/10.1002/anie.202005102.
[47] S.M. Copp, D. Schultz, S. Swasey, J. Pavlovich, M. Debord, A. Chiu, K. Olsson, E. Gwinn, Magic numbers in DNA-stabilized fluorescent silver clusters lead to magic colors, J. Phys. Chem. Lett. 5 (2014) 959–963, https://doi.org/10.1021/jz500146q.
[48] C. Dagneaux, H. Gousset, A.K. Shchyolkina, M. Ouali, R. Letellier, J. Liquier, V. L. Florentiev, E. Taillandier, Parallel and antiparallel A*A-T intramolecular triple helices, Nucl. Acids Res. 24 (1996) 4506–4512, https://doi.org/10.1093/nar/24.22.4506.
[49] D. Murphy, R. Eritja, G. Redmond, Monitoring denaturation behaviour and comparative stability of DNA triple helices using oligonucleotide-gold nanoparticle conjugates, Nucl. Acids Res. 32 (2004), https://doi.org/10.1093/nar/gnh065.
[50] Z.-L. Zhang, Y.-Y. Wu, K. Xi, J.-P. Sang, Z.-J. Tan, Divalent ion-mediated DNA-DNA interactions: a comparative study of triplex and duplex, Biophys. J. 113 (2017) 517–528, https://doi.org/10.1016/j.bpj.2017.06.021.
[51] J. Muñoz, J.L. Gelpí, M. Soler-López, J.A. Subirana, M. Orozco, F.J. Luque, Can divalent metal cations stabilize the triplex motif? Theoretical study of the interaction of the hydrated Mg^{2+} cation with the G-G·C triplet, J. Phys. Chem. B. 106 (2002) 8849–8857, https://doi.org/10.1021/jp026096w.
[52] I. Puigdomènech, E. Colàs, M. Grivé, I. Campos, D. García, A tool to draw chemical equilibrium diagrams using SIT: Applications to geochemical systems and radionuclide solubility, in: Materials Research Society Symposium Proceedings, 2014, pp. 111–116. https://doi.org/10.1557/opl.2014.635.
[53] S.W. Yang, T. Vosch, Rapid detection of microRNA by a silver nanocluster DNA probe, Anal. Chem. 83 (2011) 6935–6939, https://doi.org/10.1021/AC201903N.
[54] X. Xia, Y. Hao, S. Hu, J. Wang, Hairpin DNA probe with 5′-TCC/CCC-3′ overhangs for the creation of silver nanoclusters and miRNA assay, Biosens. Bioelectron. 51 (2014) 36–39, https://doi.org/10.1016/j.bios.2013.07.036.
[55] L. Feng, L. Wu, F. Xing, L. Hu, J. Ren, X. Qu, Novel electrochemiluminescence of silver nanoclusters fabricated on triplex DNA scaffolds for label-free detection of biothiols, Biosens. Bioelectron. 98 (2017) 378–385, https://doi.org/10.1016/j.bios.2017.07.016.
[56] T. Li, N. He, J. Wang, S. Li, Y. Deng, Z. Wang, Effects of the i-motif DNA loop on the fluorescence of silver nanoclusters, RSC Adv. 6 (2016) 22839–22844, https://doi.org/10.1039/C5RA22489F.